

## ON THE (MIS)INTERPRETATION OF THE SCATTERING POLARIZATION SIGNATURES IN THE CA II 8542 Å LINE THROUGH SPECTRAL LINE INVERSIONS

REBECCA CENTENO,<sup>1</sup> JAIME DE LA CRUZ RODRÍGUEZ,<sup>2</sup> AND TANAUSÚ DEL PINO ALEMÁN<sup>3</sup>

<sup>1</sup>High Altitude Observatory (NCAR), 3080 Center Green Dr., Boulder, CO, USA

<sup>2</sup>Institute for Solar Physics, Dept. of Astronomy, Stockholm University, AlbaNova University Centre, SE-10691 Stockholm, Sweden.

<sup>3</sup>Instituto de Astrofísica de Canarias, C. Vía Láctea s/n, La Laguna, Tenerife, Spain.

(Received July 1, 2016; Revised September 27, 2016; Accepted June 9, 2021)

Submitted to ApJ

### ABSTRACT

Scattering polarization tends to dominate the linear polarization signals of the Ca II 8542 Å line in weakly magnetized areas ( $B \lesssim 100$  G), especially when the observing geometry is close to the limb. In this paper we evaluate the degree of applicability of existing non-LTE spectral line inversion codes (which assume that the spectral line polarization is due to the Zeeman effect only) at inferring the magnetic field vector and, particularly, its transverse component. To this end, we use the inversion code STiC to extract the strength and orientation of the magnetic field from synthetic spectropolarimetric data generated with the Hanle-RT code. The latter accounts for the generation of polarization through scattering processes as well as the joint actions of the Hanle and the Zeeman effects. We find that, when the transverse component of the field is stronger than  $\sim 80$  G, the inversion code is able to retrieve accurate estimates of the transverse field strength as well as its azimuth in the plane of the sky. Below this threshold, the scattering polarization signatures become the major contributors to the linear polarization signals and often mislead the inversion code into severely over- or under-estimating the field strength. Since the line-of-sight component of the field is derived from the circular polarization signal, which is not affected by atomic alignment, the corresponding inferences are always good.

*Keywords:* solar magnetic fields

## 1. INTRODUCTION

Spectropolarimetry, the science of measuring the intensity and polarization of light as a function of wavelength, is a very powerful tool for remote sensing of thermodynamic and magnetic properties of astrophysical plasmas.

There are several physical mechanisms that can generate polarization in spectral lines. They are all related to the lack of symmetry in the absorption and excitation mechanisms of the atom. The mere presence of spectral line polarization tells us something about the conditions of the plasma where the light was emitted or absorbed. The subtleties of the intensity and polarization spectra encode a wealth of information about how the atoms were excited, and thus about the conditions dominating the atmosphere where the observed radiation was generated.

A spectral line arises from the absorption or emission of a photon when an electron transitions from one bound atomic (or molecular) energy level to another. These energy levels are, in general, degenerate. In the presence of an external magnetic field, these magnetic sub-levels (represented by the magnetic quantum number  $M$ ) split and the degeneracy is broken, leading to a wavelength shift between the  $\pi$  ( $\Delta M = 0$ ) and  $\sigma$  ( $\Delta M = \pm 1$ ) components of the spectral line. The splitting of the energy levels is, in general, proportional to the magnetic field strength, and this polarization mechanism is commonly known as the Zeeman effect. If the magnetic field is very weak (relative to the width of the spectral line), or absent, the wavelength shift of the magnetic sub-levels is very small and the ensuing polarization signatures are negligible. This is especially true for the linear polarization signatures of chromospheric lines, which scale with the square of the ratio between the Zeeman splitting and the line widths, instead of linearly, as the circular polarization features do.

But even in the absence of magnetic fields, there are other mechanisms that can generate polarization in spectral lines. When the magnetic sub-levels of a given energy level are unevenly populated (i.e. atomic level polarization), this results in an imbalance between the number of  $\pi$  and  $\sigma$  transitions per unit volume and time, which leads to emergent polarization signatures without the need to invoke a wavelength shift (see [Trujillo Bueno \(2001\)](#) for a short introductory review to scattering polarization and the Hanle effect and [Landi Degl'Innocenti & Landolfi \(2004\)](#) for a detailed explanation of the origin of polarization in spectral lines). The population imbalance and quantum coherence among the degenerate magnetic sublevels, known as atomic level polarization, lead to an imbalance between the rates of different  $|\Delta M|$  transitions, which, in turn, produces emergent linear polarization signals, commonly referred to as “scattering polarization”.

In the Sun’s atmosphere, the most common mechanism for creating atomic level polarization is the so-called optical pumping, that is, the anisotropic illumination of the atoms leads to selective emission or absorption of the different spectral line components, and to scattering linear polarization, without the need for a magnetic field. Elastic collisions have a strong depolarizing effect, and tend to equalize the populations of the magnetic sublevels. So for this mechanism to be effective, the radiative transitions have to dominate the atomic excitation and deexcitation processes. In the rarefied environment of the chromosphere, collisions are infrequent and the radiation is weakly coupled to the local thermodynamic conditions (this is commonly referred to as non Local Thermodynamic Equilibrium or non-LTE). This sets a perfect stage for optical pumping to act effectively, creating atomic level polarization that leads to the generation of polarization signatures in spectral lines in the absence of an external magnetic or electric field. In chromospheric quiet Sun regions, where the magnetic fields are weak and the Zeeman effect generates small polarization signatures, the linear polarization of chromospheric lines is typically dominated by scattering processes ([Manso Sainz & Trujillo Bueno 2010, 2003](#)).

The Hanle effect is the relaxation of the atomic level coherences due to the presence of a magnetic field. When a magnetic field is present, the emergent scattering polarization signals will change with respect to the zero-field case, leaving a measurable imprint on the polarization spectrum. The Hanle effect is typically sensitive to relatively weak magnetic field strengths (depending on the spectral line) and allows us to access regimes where the Zeeman effect does not have useful diagnostic capabilities.

The Ca II 8542 Å line has been deemed one of the most promising lines for chromospheric magnetic field diagnostics ([Lagg et al. 2017; Quintero Noda et al. 2016, 2017](#)) due to its accessibility from ground-based observations and the relative ease of its interpretation – this is, when modeling it, it is safe to assume complete redistribution ([Uitenbroek 1989](#)), ignore non-equilibrium ionization effects ([Wedemeyer-Böhm & Carlsson 2011](#)), and full 3-D radiative transfer computations are unnecessary in certain scenarios ([de la Cruz Rodríguez et al. 2012](#)). **It is of interest to note that neglecting 3D radiative transfer effects can have a large impact on the scattering polarization signals of this and other spectral lines (see [Bestard et al. 2021](#), for an analysis of their impacts on Ca I 4227Å).** The presence of horizontal inhomogeneities in the physical properties of the Sun’s atmosphere can also

break the axial symmetry of the radiation field, fueling an additional source of atomic level polarization. Štěpán and Trujillo Bueno (2016) quantified the error in the emergent linear polarization of Ca II 8542 Å when neglecting said horizontal inhomogeneities, and concluded that it could be as large as the linear polarization amplitudes themselves. This study was carried out on the polarization signals emerging from a high resolution quiet Sun radiation magneto-hydrodynamic simulation, and probably represents an upper bound for these scattering polarization signals. Spatial degradation of the spectral profiles and stronger magnetic fields will likely render these 3-D radiative transfer effects less important.

Despite it being commonly used to extract information about the chromospheric magnetic field, whether the interpretation is done by applying the weak field approximation (WFA, see, for instance Centeno 2018; Kuridze et al. 2019; Morosin et al. 2020) or using non-LTE spectral line inversion codes (de la Cruz Rodríguez et al. 2019; Socas-Navarro et al. 1998; Milić & van Noort 2018; Ruiz Cobo et al. 2021), these diagnostic tools do not account for the physics of scattering polarization nor its modification via the Hanle effect. However, scattering polarization signatures typically dominate the linear polarization profiles of Ca II 8542 Å in weak field areas (Manso Sainz & Trujillo Bueno 2010, 2003), particularly close to the limb, where the observing geometry maximizes these polarization signatures. When combined with the enhancing effect of shocks, the linear polarization signatures can reach amplitudes of up to 1% of the continuum intensity (Carlin et al. 2012, 2013), which would dominate over Zeeman signatures induced by magnetic fields in the hecto-gauss range.

To date, the only spectral line inversion codes that account for the physics of scattering polarization and the combined action of the Hanle and Zeeman effects are limited to the interpretation of some neutral He lines, where computing the radiative transfer in a slab of constant properties can be a suitable approximation (see, for instance Asensio Ramos et al. 2008).

This work attempts to evaluate the inaccuracy in the chromospheric magnetic field values retrieved from non-LTE inversions of the Ca II 8542 Å line when neglecting the scattering polarization signals and their modification due to the Hanle effect. Section 2 describes the computer codes and numerical setups used to synthesize and invert the spectral lines. In section 3 we present the analysis of the inversion results, followed by some brief thoughts and conclusions in section 4.

## 2. SYNTHESIS AND INVERSION OF SPECTRAL LINES

Purely a numerical experiment, this work aims at quantifying the biases incurred by non-LTE spectral line inversion codes when analyzing Ca II 8542 Å Stokes spectra. Currently, the non-LTE spectral line inversion codes capable of interpreting the spectral line radiation in the Ca II IR triplet do not account for the generation of polarization induced by scattering processes and its modification due to the Hanle effect. There are, however, forward modeling radiative transfer software packages that account for the subtle quantum-mechanical effects responsible for these processes, which can realistically model the polarization signatures of Ca II 8542 Å.

Hanle-RT (see, for instance, del Pino Alemán et al. 2016) is a 1.5-D radiative transfer code able to solve the polarized radiation transfer problem in a plane-parallel geometry, under non-LTE conditions, for a multi-term or multi-level atom in the presence of an arbitrary magnetic field, taking into account the effects of partial frequency redistribution (PRD), as well as the contribution of inelastic and elastic collisions. **The rate of depolarizing elastic collisions with neutral hydrogen are the result of ab initio quantum mechanical calculations by (Manso Sainz et al. 2014).** Spectral line polarization is generated by means of scattering processes as well as by the combined action of the Hanle and Zeeman effects.

### 2.1. *Synthesis*

The Hanle-RT code was used to synthesize the Stokes profiles of the Ca II 8542 Å line in a number of magnetic field scenarios and observing geometries. The spectra were synthesized in the 1-D semi-empirical C model atmosphere of Fontenla et al. (1993), hereafter, FALC. Constant magnetic fields with varying strengths (from 0 to 100 G in steps of 20 G and from 100 G to 1000 G in steps of 100 G), horizontal with respect to the local solar surface, were introduced ad-hoc in the model to generate the corresponding Zeeman/Hanle polarization signatures. The spectra were generated for lines-of-sight (LOS) with five different heliocentric angles ( $\theta$ ), from disk center to close to the limb ( $\mu = 1, 0.9, 0.6, 0.5, 0.1$ , where  $\mu = \cos\theta$ ). In all geometries, the magnetic field was kept horizontal to the local solar surface, so the angle between the magnetic field direction and the LOS adopts different values (and so does the ratio of linear to circular Zeeman-induced polarization from the observer's perspective). Figure 1 depicts three of the LOS

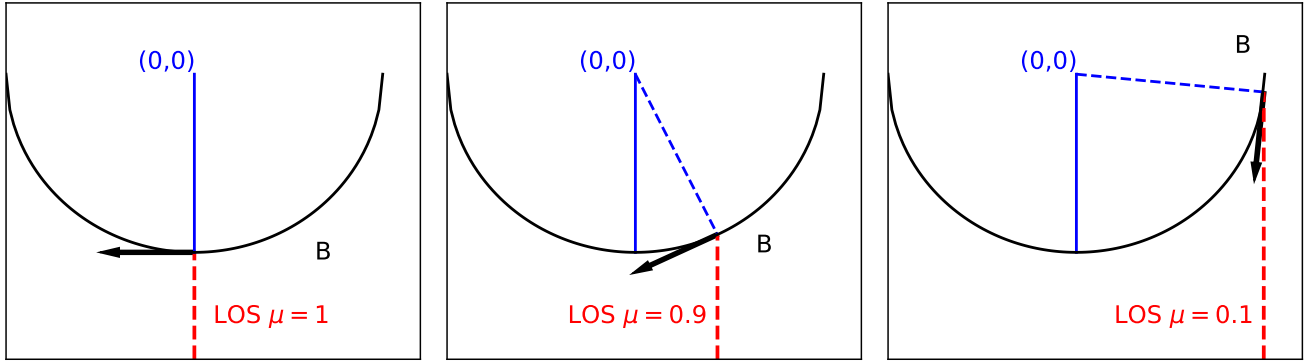


**Figure 1.** Representation of three of the five LOS geometries used in the Hanle-RT forward modeling calculations ( $\mu = 1$ ,  $\mu = 0.9$  and  $\mu = 0.1$  shown here). This figure shows a top view of a cross-section through the Sun's equator, where  $(0,0)$  represents the center of the Sun. The magnetic field vector,  $\vec{B}$ , is always tangent to the solar surface, and its LOS component points towards the observer for the observing geometries away from the disk center. The Sun's equator, the magnetic field and the LOS are in the same plane.

geometries listed above, where the black arrow represents the magnetic field vector, always tangential to the solar surface, and the red dashed line shows the line-of-sight.

The atomic model of Ca II used in this work has five bound energy levels as well as the Ca III continuum, allowing for 5 bound-bound radiative transitions (i.e. the Ca II H & K lines in the near UV and the Ca II infrared triplet, see Fig. 1 in Centeno 2018). Ca II 8542 Å is a magnetically sensitive line that arises from the transition between the  $3^2D_{5/2}$  and the  $4^2P_{3/2}$  levels. Both in the Hanle-RT synthesis as well as in the spectral line inversion, the IR triplet is computed assuming complete frequency redistribution (CRD), whilst the H & K UV lines are treated in PRD accounting for Raman scattering (also referred to as “cross-redistribution” in some works) from the IR triplet to the UV doublet. The spectral lines were synthesized on a regular wavelength grid with a spectral sampling of 1 mÅ and a coverage that spanned  $\pm 1.2$  Å from the line core. No additional broadening mechanisms (aside from the natural, thermal and collisional broadenings) were included in the calculations, which allowed for a fair amount of continuum in the polarization spectra.

Two sets of synthetic Stokes spectra were computed for each magnetic field strength and each observing geometry, one in which the linear polarization signatures were a consequence of scattering phenomena as well as the joint actions of the Hanle and Zeeman effects, and another one in which the atomic level polarization was “turned off” and only the signals due to the Zeeman effect were permitted. This allowed us to evaluate the performance of the spectral line inversion of purely Zeeman-induced signatures against the inversion of the more realistic scenario including scattering polarization and the Hanle effect. The total number of synthetic Stokes profiles is 150 (15 values of the field strength for 5 observing geometries and 2 calculation modes - with and without atomic level polarization).

Figure 2 shows a few examples of the synthetic Stokes profiles for several field strengths and observing geometries. As expected, the Stokes spectra for the LOS with  $\mu = 0.1$  (the two examples on the right side of the figure) show the largest differences between the Zeeman-only case (blue solid line) and the full calculation with scattering polarization (magenta dots). This is because observing geometries very close to the limb favor larger contributions of scattering polarization to the Stokes profiles. Note that for the disk center geometry ( $\mu = 1.0$ ), V/I is always zero, because the magnetic field is tangential to the surface and therefore transverse to the line-of-sight (see Fig. 1). In all other geometries, there is a V/I signal as long as the magnetic field is non-zero. Stokes I and Stokes V are not affected by this form of atomic level polarization (atomic alignment), so the Zeeman-only and full calculation profiles look identical.

## 2.2. Inversion

As stated earlier, there is currently no non-LTE spectral line inversion code capable of treating the physical processes that lead to atomic level polarization and the Hanle effect in the Ca II 8542 Å line. In order to assess how “standard” non-LTE spectral line inversion codes interpret the polarized signatures due to these subtle quantum-mechanical effects, we inverted the synthetic Hanle-RT profiles with the Stockholm inversion Code (STiC, de la Cruz Rodríguez et al. 2019, 2016) and compared the inversion results to the magnetic field of the model used to generate the original spectra.

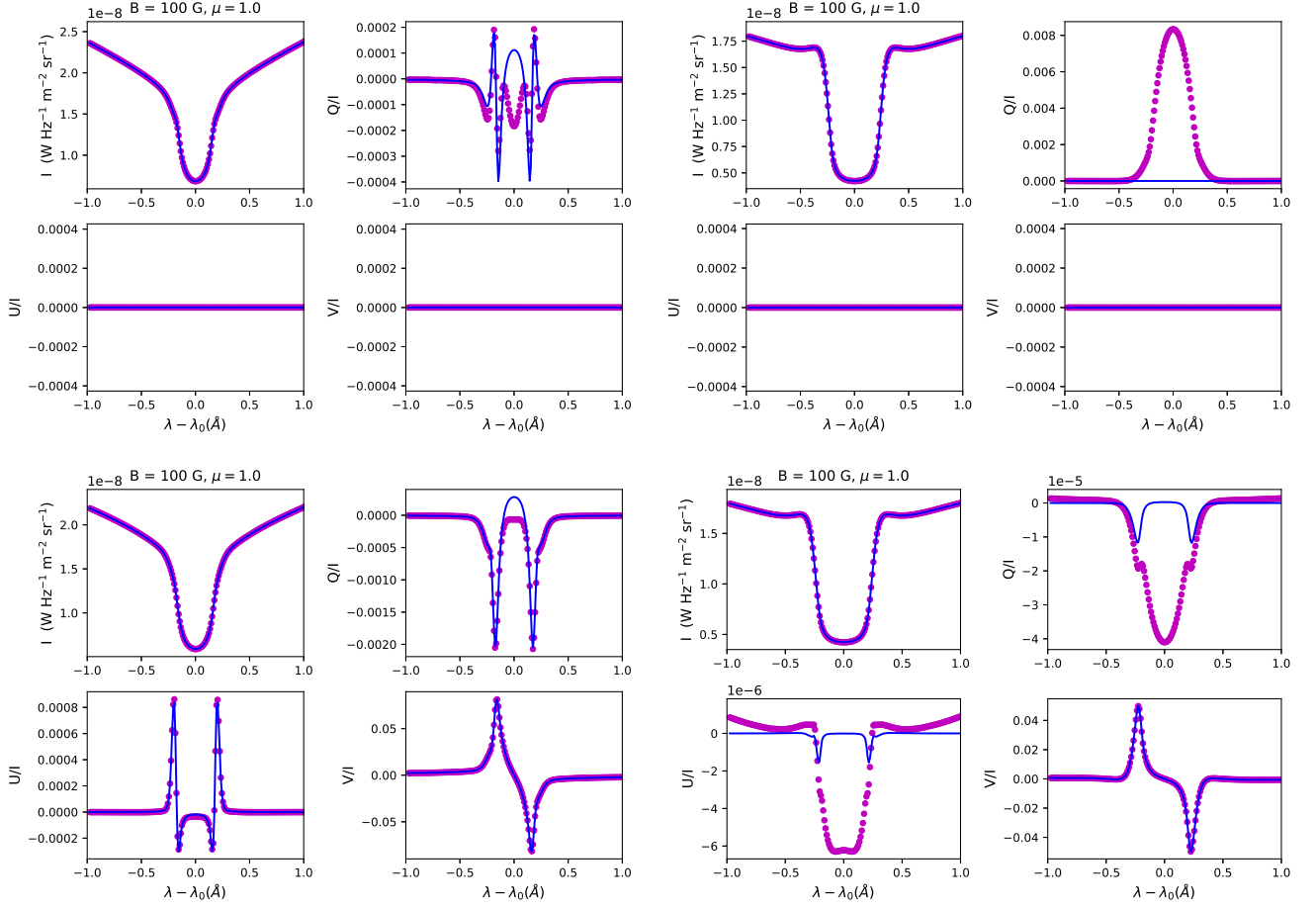


**Figure 2.** Examples of sets of synthetic Stokes profiles for different magnetic field strengths and different observing geometries. The magenta dots correspond to the profiles computed taking into account scattering polarization and the joint action of the Hanle and Zeeman effects, whilst the blue solid line corresponds to the calculations where only Zeeman-induced polarization was permitted. The field strength and the observing geometry,  $\mu$ , are labeled at the top of each Stokes I panel.

STiC is a parallelized non-LTE full-Stokes spectral line inversion code that uses a modified version of the Rybycki and Hummer radiative transfer code (RH, [Uitenbroek 2001](#)) to solve for the atomic population densities assuming statistical equilibrium in a plane-parallel atmosphere. The code can account for PRD effects ([Leenarts et al. 2012](#)), which are important for the modeling of many chromospheric lines. The polarized radiative transfer equation is solved using cubic Bezier solvers ([de la Cruz Rodríguez & Piskunov 2013](#)). The inversion engine of STiC is based on a Levenberg-Marquardt algorithm ([Press et al 1992](#)), and includes an equation of state extracted from the Spectroscopy Made Easy (SME, [Piskunov & Valenti 2017](#)) code. Polarization is exclusively generated by the Zeeman effect, therefore STiC cannot account for polarization due to scattering processes and its modification via the Hanle effect.

As in the synthesis, the Ca II model atom used in the inversions contains 5 bound energy levels and the Ca III continuum, which allows for the bound-bound radiative transitions of Ca II H & K and the Ca IR triplet. As in the previous section, the H & K lines are treated in the PRD regime, while the IR triplet is computed assuming CRD.

The inversions were carried out in two cycles, following the strategy of [Vissers et al. \(2021\)](#), with 4 nodes for the temperature in the first cycle and 7 in the second cycle. The number of nodes for the rest of the parameters stayed constant throughout the 2 cycles, with 3 for the microturbulent velocity, and one for each one of the remaining physical parameters (the LOS velocity, the LOS component of the magnetic field, the transverse component of the magnetic field and its azimuth in the plane of the sky). In the case of the viewing angle with  $\mu = 0.1$ , additional nodes for the temperature and the microturbulent velocity were needed in the second cycle in order to obtain a good fit to the Stokes I profile. However, STiC implements a regularization of the merit function that minimizes artifacts

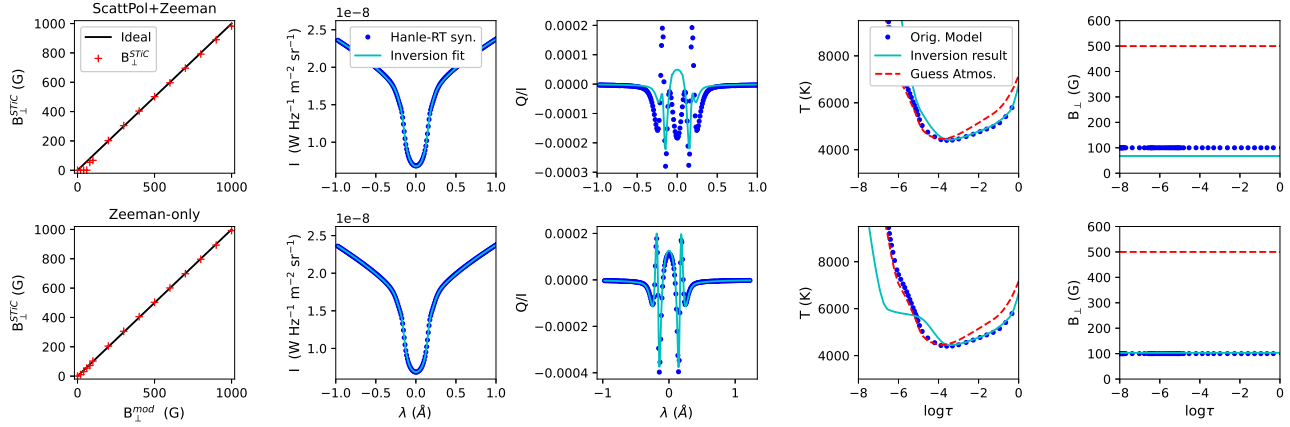


**Figure 3.** Inversion results for the LOS with  $\mu = 1$ . The top row shows results for the cases in which atomic polarization was accounted for, while the bottom row concerns itself with the Zeeman-only case. The first column shows the retrieved magnetic field vs. the model value, where the solid line represents the one-to-one expected correspondence. The second and third columns show the fits (cyan lines) to the Hanle-RT Stokes I and Q/I (blue dots) for the case of a magnetic field of  $\sim 100$  G. The last two columns present the retrieved temperature and magnetic field (cyan line) as a function of optical depth, and how they compare to the model used for the Hanle-RT synthesis (blue dots), as well as the initial guess for the inversion (red line).

in the atmospheric gradients that result from the excess freedom in the parameters of the model atmosphere (see de la Cruz Rodríguez et al. 2019, for details).

The initial guess model atmosphere was the same for all inversions. It consisted of a version of the FAL-C model with a perturbed temperature profile and a constant value for the LOS velocity and the magnetic field vector. Each set of Stokes spectra was paired with a set of weights to ensure a good inversion fit for all Stokes parameters simultaneously (Del Toro Iniesta & Ruiz Cobo 2016). The inversion weights are a set of 4 values used to emphasize or de-emphasize the relative importance of a given Stokes parameter with respect to Stokes I in the evaluation of the merit function,  $\chi^2$ , that the inversion algorithm is trying to minimize (see explanation in Centeno et al. 2014, for instance):

$$\chi^2 = \sum_s \frac{w_s^2}{\sigma_s} \sum_{\lambda} [I_s^{\text{OBS}}(\lambda) - I_s^{\text{SYN}}(\lambda)]^2 \quad (1)$$

where the weights,  $w_s$ , were chosen to approximately equalize the amplitudes of the synthetic Hanle-RT Stokes Q, U and V to that of Stokes I. In this expression,  $I^{\text{OBS}}$  represents the Hanle-RT Stokes spectra to be inverted and  $I^{\text{SYN}}$  represents the best fit found by the STiC inversion code.  $\sigma_s$  is the expected noise of each one of the Stokes parameters. The data that we were inverting were noiseless, so we artificially set to  $\sigma_s \sim 10^{-3}$  times the continuum intensity to indicate to STiC the magnitude of the acceptable error in fitting Stokes I. The indices  $s$  and  $\lambda$  run through the 4 Stokes parameters and the wavelength, respectively. Note that the merit function inside the STiC code has additional terms that apply the regularization scheme and the normalization of  $\chi^2$ .

### 3. ANALYSIS

#### 3.1. Disk center, $\mu = 1$

Figure 3 summarizes the results for the observing geometry with  $\mu = 1.0$ . The top row shows inversion results for the profiles computed with scattering polarization and the joint action of the Hanle and Zeeman effects, whilst the bottom row presents the results for the Zeeman-only case. The left-most column compares the values of the horizontal field retrieved by the STiC inversion,  $B_{\perp}^{\text{STiC}}$ , to the field in the model,  $B_{\perp}^{\text{mod}}$  (with which the synthetic Hanle-RT profiles were generated). The retrieved magnetic field values in the Zeeman-only case (bottom) are always extremely close to the truth (black solid line). The initial atmospheric guess as well as the choice of weights for the Stokes parameters impact the solution to some degree, resulting in very small deviations from the truth. For the case of the full calculation (top) the agreement is remarkable and not qualitatively different to the Zeeman-only case when the field strength is above  $\sim 100$  G. Significant disagreements between the retrieved field values and the expected ones

appear below this threshold. In this regime, the signatures of the Hanle effect alter the shape of the linear polarization profiles significantly, resulting in a misinterpretation from the STiC code.

The second and third columns show the best fits found by the inversion (cyan line) to the Hanle-RT Stokes I and Q/I (blue dots), synthesized for a magnetic field of 100 G. In this particular geometry, U/I and V/I are exactly zero. It is obvious that the STiC inversions are not able to fit the signatures characteristic of the Hanle effect (Q/I panel in top row), while it does a good job at fitting the Zeeman-only profile (bottom row). Despite the misfit of the former, STiC is still able to infer an approximate value of the magnetic field by virtue of attempting to fit the width and amplitude of the Q/I profile. It is worth noting that, in general, the quality of the fits becomes increasingly better as the field strength increases and the Hanle contribution becomes less and less important. Below 100 G, the inversion fits are poor and the inferred magnetic field values are rather inaccurate.

Columns 4 and 5 compare the retrieved temperature and horizontal magnetic field stratifications as a function of optical depth (solid cyan lines) to the model atmosphere used for the synthesis (blue dots). The disagreements between the original and the inverted temperature profiles are partly due to a degeneracy between this physical quantity and the microturbulent velocity. This degeneracy can be mitigated by carrying out simultaneous inversions of multiple spectral lines with different sensitivities to temperature (see, for instance, [de la Cruz Rodríguez et al. 2019](#); [da Silva Santos et al. 2018](#)). That said, the discrepancies are larger at optical depths where Ca II 8542 Å lacks sensitivity to the temperature, especially above  $\log\tau = -5.5$  ([Quintero Noda et al. 2016](#)). In the regions of the atmosphere where the Ca II 8542 Å line should have sensitivity to the temperature, some of the discrepancy between the original model and the inversion results comes from the fact that the Hanle-RT syntheses were carried out in the FALC model atmosphere with electron density and hydrogen populations calculated in non-LTE. For the inversion, on the other hand, the STiC code was set up to solve the statistical equilibrium for the Ca II atom only, while the H populations and electron densities were computed internally under the assumption of LTE. Additional sources of discrepancy, more difficult to quantify, stem from the differences between the Hanle-RT and STiC codes in the formulation of the equation of state, the algorithm that computes the formal solution of the equation of transfer, and other factors that might affect the convergence of the statistical equilibrium. In these last two columns of Fig. 3, the red line shows the guess model atmosphere used to initialize the inversion.

### 3.2. Other geometries

As we move to observing geometries away from the disk center, the magnetic field presents both a longitudinal as well as a transverse component in the LOS reference frame. This leads to the appearance of Stokes V signals exclusively due to the longitudinal Zeeman effect. Furthermore, the fraction of Zeeman-induced linear polarization becomes smaller and the effects of scattering polarization become more important as the heliocentric angle of the “observation” increases (i.e.  $\mu$  decreases).

Figure 4 shows a comparison between the components of the vector magnetic field retrieved by the STiC inversions and those used for the Hanle-RT syntheses, for the LOS away from the disk center. The left column corresponds to the inversion of Zeeman-only profiles whilst the right column depicts the results for the full forward calculation with atomic polarization.

The top row quantifies the relative (percent) difference between the inferred ( $B_{\perp}^{\text{STiC}}$ ) and model ( $B_{\perp}^{\text{mod}}$ ) values of the transverse magnetic field, as a function of the model value. The x-axis is on a logarithmic scale to allow the reader to clearly see the results at low field strengths ( $B_{\perp}^{\text{mod}} < 100$  G), and each line of sight is represented by a colored symbol. For transverse magnetic field strengths above 80 G, the inversion results are always within 5% of the true value, regardless of whether STiC is interpreting the spectra from the full scattering polarization calculation or the Zeeman-only signals. Below 80 G (marked by the vertical gray line), the inferences derived from the spectra with scattering polarization (right) start to deviate significantly from the true values, whilst in the case of the Zeeman-only signals (left), the inversion inferences are still accurate. The middle row shows the difference between the inferred and the model magnetic field azimuths (in degrees) as a function of  $B_{\perp}^{\text{mod}}$ . Just like in the case of the horizontal field strength, the inferences from the scattering polarization signatures become less reliable below the 80 G mark.

The bottom row presents the inversion results for the longitudinal component of the magnetic field,  $B_{\parallel}^{\text{STiC}}$ , and how they compare to the model values ( $B_{\parallel}^{\text{mod}}$ ). Because the atomic level polarization only carries atomic alignment, it does not affect the circular polarization signals, which are exclusively due to the Zeeman effect. Therefore, the Stokes V signals are correctly interpreted by STiC, and the  $B_{\parallel}^{\text{STiC}}$  inferences are always rather accurate.

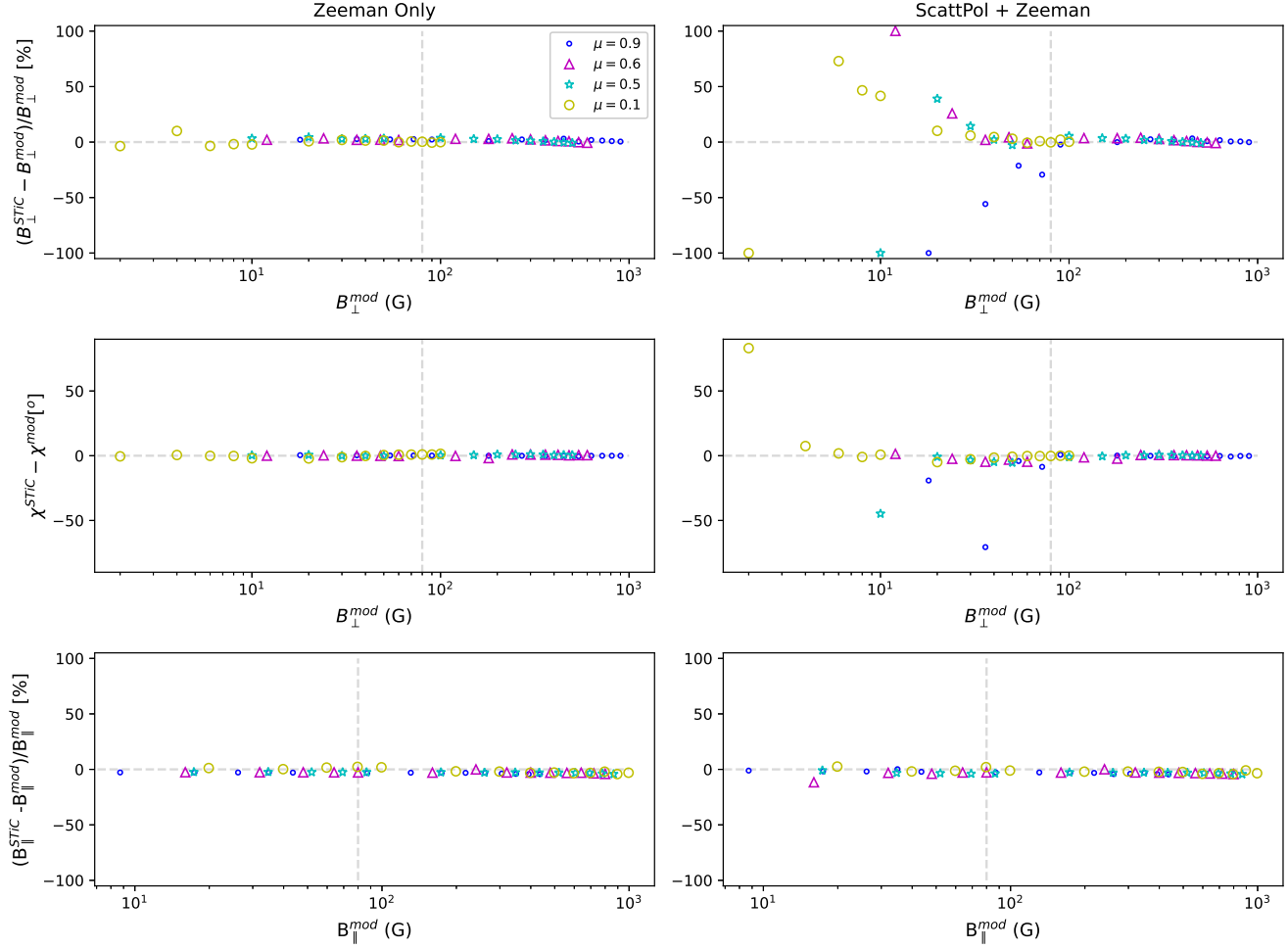


**Figure 4.** Inversion results for observing geometries away from the disk center. The panels show the relative (percent) differences between the magnetic field values retrieved by the STiC inversions and those in the model atmospheres used for the Hanle-RT syntheses. Left and right correspond, respectively, to the Zeeman-only and the full calculation with atomic polarization cases. The top two rows show the results for the strength and the azimuth of the transverse component of the magnetic field, while the bottom panels present the results for the LOS magnetic field.

### 3.3. The case of $\mu = 0.1$

Special consideration should be given to the case of the LOS with  $\mu = 0.1$ . This corresponds to the observing geometry closest to the limb, and therefore has the smallest transverse magnetic fields in the observer's reference frame ( $B_{\perp}^{\text{mod}}$  ranging from 0 to 100 G). Also, the linear polarization profiles in this scenario will be the most affected by scattering polarization and the Hanle effect.

Figure 5 shows the best inversion fits for the case  $B^{\text{mod}} = 200$  G in the observing geometry  $\mu = 0.1$ . In the LOS reference frame, this corresponds to a transverse magnetic field of  $B_{\perp}^{\text{mod}} = 20$  G and a LOS component of  $B_{\parallel}^{\text{mod}} = 199$  G. The top row corresponds to the full calculation, including scattering polarization and the Hanle effect, while the bottom row shows the results for the Zeeman-only calculations. The open circles represent the synthetic profiles calculated with Hanle-RT (from left to right,  $I$ ,  $Q/I$ ,  $U/I$ ,  $V/I$ ) while the cyan solid line shows the best fit found by the STiC inversion code. This figure epitomizes how the inversion code interprets the signatures introduced by atomic polarization and the Hanle effect in the linear polarization profiles. In particular, the second panel of the top row shows the Stokes  $Q/I$  profile affected these subtle quantum mechanical effects (magenta circles), which is to be compared to its Zeeman-only counterpart in the bottom row (blue circles). In both cases, the best fits found by the inversion code (cyan lines) look rather similar, and yield comparable values of the transverse magnetic field: the inversions of the Zeeman-only case yields 20.2 G, whilst the full calculation results in 22.0 G. The model value was

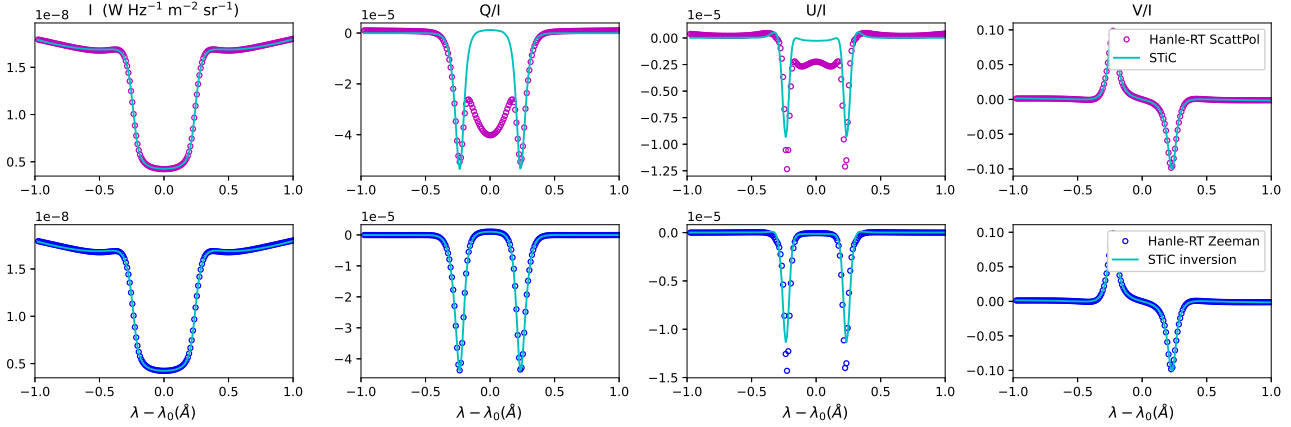


**Figure 5.** Inversion fits for the case of  $B_{\perp}^{\text{mod}} = 200$  G and observing geometry with  $\mu = 0.1$ . The open circles represent the Hanle-RT synthetic profiles, while the cyan line shows the best fit found by the inversion code. The top row shows the case of the full calculation while the bottom row corresponds to the Zeeman-only spectra.

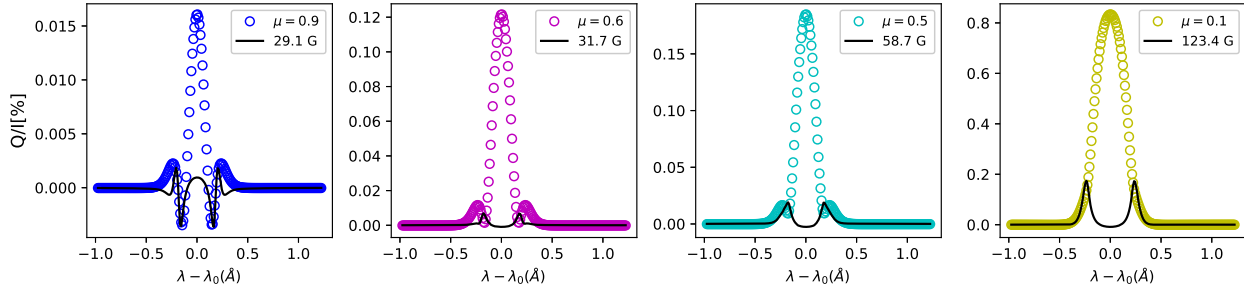


**Figure 6.** Inversion fit (black line) of  $Q/I$  for the zero-field case when scattering polarization is accounted for (open circles). STiC attempts to fit the non-magnetic scattering polarization signals as if they were of Zeeman origin, leading to non-zero inferences of the transverse component of the magnetic field (the value retrieved in each case is listed in each legend).

$B_{\perp}^{\text{mod}} = 20$  G in this case. Even though the Hanle effect strongly depolarizes the  $\pi$  component of the Stokes  $Q/I$  signal, there might be enough information in the inner wings for STiC to extract information about the magnetic field through the Zeeman effect. The resulting  $B_{\perp}^{\text{STiC}}$  is only over-estimated by 10% in this case.

#### 3.4. The zero-field case

The case of the full calculation for  $B = 0$  G misleads the inversion code, since the purely scattering polarization Stokes  $Q$  signals are interpreted by STiC as Zeeman-induced transverse magnetic fields of tens to a hundred gauss. Figure 6 shows the STiC fits (black solid lines) to the Hanle-RT  $Q/I$  profiles (open circles) for the case of the full calculation with  $B = 0$  G. From left to right, the observing geometry goes from  $\mu = 0.9$  to  $\mu = 0.1$ . As the figure suggests, STiC is not able to fit the  $Q/I$  profiles, yet it attempts to mimic the scattering polarization signals in order to minimize the merit function that drives the inversion algorithm. This leads to non-zero values of the magnetic field, which in the case of the most extreme observing geometry yields  $B_{\perp}^{\text{STiC}} \sim 120$  G.

#### 4. CONCLUSIONS

Most spectral line inversion codes that are able to interpret chromospheric spectra formed under non-LTE conditions do not account for all the physical processes that can generate polarization in these lines. Although the Zeeman effect is taken into account in these codes (de la Cruz Rodríguez et al. 2019; Socas-Navarro et al. 1998; Milić & van Noort 2018; Ruiz Cobo et al. 2021), the physics for the generation and transfer of polarization due to scattering and its modification via the Hanle effect are not. This work assesses the errors made by one of these inversion codes (STiC) when interpreting the polarization signatures of Ca II 8542 Å.

To estimate the errors incurred by STiC when interpreting the Ca II 8542 Å spectra we invert sets of Stokes profiles synthesized with the Hanle-RT code in the FALC model atmosphere with ad-hoc magnetic fields of different strengths. Hanle-RT computes the spectral line polarization generated by scattering processes as well as its modification due to the combined actions of the Hanle and Zeeman effects. The spectra were synthesized simulating 5 observing geometries, from disk center ( $\mu = 1$ ) to close to the solar limb ( $\mu = 0.1$ ).

We find that, for most field strengths and observing geometries, STiC does a good job at retrieving both the longitudinal and the transverse components of the magnetic field. Even when the amplitude of the scattering polarization and Hanle signatures are comparable to that of the Zeeman signature in the linear polarization profiles, STiC is able to retrieve the transverse component of the magnetic field with remarkable accuracy, over-estimating its value by only a few percent. When the transverse magnetic field component is weaker than 80 G, the scattering polarization and Hanle signatures start dominating over the Zeeman-induced signals. Naturally, STiC is not able to reproduce the spectral signatures induced by scattering polarization and the Hanle effect, leading to errors in the retrieved transverse component of the magnetic field and its azimuth in the plane of the sky.

In the case where the model magnetic field is  $B^{\text{mod}} = 0$  G, and polarization signatures are exclusively due to scattering processes, STiC still attempts to fit the linear polarization by interpreting it as a Zeeman signal. This leads to spurious transverse magnetic field values, which in the case of  $\mu = 0.1$  is just over 120 G. However, by visually inspecting the original spectra as well as the inversion fits, it is possible to determine that the agreement is poor and that the inversion results are questionable.

This is a relatively simple experiment that only addresses spectral profiles synthesized in a 1-D static semi-empirical model atmosphere with constant magnetic fields in the absence of noise in the Stokes parameters. **The 1-dimensional nature of this study omits, by design, the effects of spatial inhomogeneities and horizontal radiative transfer on the atomic level polarization. This likely leads to an under- or over-estimate of the typical linear polarization signals expected in very quiet areas of the (real) Sun, which will become less important in more strongly magnetized regions.** Moreover, as mentioned in the introduction, strong velocity gradients can lead to much larger scattering polarization signatures in observing geometries close to the limb. The interpretation of such signals with a non-LTE inversion code could lead to larger errors in the retrieved magnetic field values. Nevertheless, this work provides a first attempt at setting a threshold for the applicability of non-LTE spectral line inversion codes, and shows that, when the contribution of scattering polarization to the linear polarization signals is smaller than that of its Zeeman-induced counterpart, the inversion results are as accurate as when the polarization signals are due to the Zeeman effect only.

This material is based upon work supported by the National Center for Atmospheric Research, which is a major facility sponsored by the National Science Foundation under Cooperative Agreement No. 1852977. This project has received funding from the European Research Council (ERC) under the European Union’s Horizon 2020 research and innovation programme (SUNMAG, grant agreement 759548). TdPA acknowledges the funding received from the European Research Council (ERC) under the European Union’s Horizon 2020 research and innovation programme (ERC Advanced Grant agreement No 742265).

## REFERENCES

Asensio Ramos, A., Trujillo Bueno, J., & Landi Degl’Innocenti, E. 2008, *ApJ*, 683, 542.

Asensio Ramos, A., de la Cruz Rodríguez, J., Martínez González, M.J., Socas-Navarro, H., 2017, *A&A*, 599, 133.

Bestard, J.J., Trujillo Bueno, J., Štěpán, J., del Pino Alemán, T., 2021, *ApJ*, 909, 2.

Carlin, E.S., Manso Sainz, R., Asensio Ramos, A., Trujillo Bueno, J., 2012, *ApJ*, 751, 5C.

Carlin, E.S., Asensio Ramos, A., Trujillo Bueno, J., 2013, *ApJ*, 764, 40.

Centeno, R., 2018, *ApJ*, 866, 89.

Centeno, R., Schou, J., Hayashi, K., Norton, A., Hoeksema, J. T., Liu, Y., Leka, K. D., K. D., Barnes, G., 2014, *Solar Physics*, 289, 9.

da Silva Santos, J.M., de la Cruz Rodríguez, J., Leenaarts, J., 2018, *A&A*, 620, 124.

de la Cruz Rodríguez, J., Socas-Navarro, H., Carlsson, M., Leenarts, J., 2012, *A&A*, 543, 34.

de la Cruz Rodríguez, J.; Leenaarts, J.; Asensio Ramos, A., 2016, *ApJ*, 830L, 30D.

de la Cruz Rodríguez, J.; Lenaarts, J.; Danilovic, S.; Uitenbroek, H., 2019, *A&A*, 623, 74.

de la Cruz Rodríguez, J.; Piskunov, N., 2013, *ApJ*, 764, 33D.

del Pino Alemán, T., Casini, R., Manso Sainz, R., 2016, *ApJL*, 830L, 24.

Del Toro Iniesta, J.C., Ruiz Cobo, B., 2016, *Living Rev. Sol. Phys.*, 13:4.

Fontenla, J.M., Avrett, E.H., Loeser, R., 1993, *ApJ*, 406, 319.

Kuridze, D., Mathioudakis, M., Morgan, H., Oliver, R., Kleint, L., Zaqrashvili, T. V., Reid, A.; Koza, J., Lfdahl, M. G., Hillberg, T., Kukhianidze, V., Hanslmeier, A., 2019, *ApJ*, 874, 126.

Lagg, A., Lites, B.W., Harvey, J., Gosain, S., Centeno, R., 2017, *Space Science Reviews*, Volume 210, Issue 1-4.

Landi Degl'Innocenti, E., Landolfi, M., 2004, *Polarization in Spectral Lines*, Astrophysics and Space Library, Volume 307, Kluwer Academic Publishers, Dordrecht.

Leenaarts, J.; Pereira, T.; Uitenbroek, H., 2012, *A&A*, 543A, 109L.

Manso Sainz, R., Roncero, O., Sanz-Sanz, C., Aguado, A., Asensio Ramos, A., Trujillo Bueno, J., 2014, *ApJ*, 788, 2.

Manso Sainz, R., Trujillo Bueno, J., 2003, *Phys. Rev. Lett.*, 91, 111102.

Manso Sainz, R., Trujillo Bueno, J., 2010, *ApJ*, 722, 1416.

Milić, I., van Noort, M., 2018, *A&A*, 617, 24.

Morosin, R.; de la Cruz Rodríguez, J.; Vissers, G. J. M.; Yadav, R., 2020, *A&A*, 642, 210.

Pietarila, A., Socas-Navarro, H., Bogdan, T., 2007, *ApJ*, 670, 885.

Piskunov, Nikolai; Valenti, Jeff A., 2017, *A&A*, 597A, 16P.

Press, W.H., Teukolsky, S.A., Vetterling, W.T., & Flannery, B.P. , 1992, "Numerical recipes in C: The art of scientific computing". Second Edition. Cambridge University Press.

Quintero Noda, C., Shimizu, T., de la Cruz Rodríguez, J., Katsukawa, Y., Ichimoto, K., Anan, T., Suematsu, Y., 2016, *MNRAS*, 459, 3.

Quintero Noda, C., Shimizu, T., Katsukawa, Y., de la Cruz Rodríguez, J., Carlsson, M., Anan, T., Oba, T., M., Ichimoto, K., Suematsu, Y., 2017, *MNRAS*, 464, 4.

Ruiz Cobo, B., Quintero Noda, C., Gafeira, R., Uitenbroek, H., Orozco Suárez, D., Páez Mañá, E., 2021, *A&A*, submitted.

Socas-Navarro, H., Trujillo Bueno, J., Ruiz Cobo, B., 1998, *ApJ*, 507, 470.

Štěpán, J., Trujillo Bueno, J., 2016, *ApJ*, 826L, 10S.

Trujillo Bueno, J., 2001, in "Advanced Solar Polarimetry: Theory, Observations and Instrumentation", Proc. 20th International Sac. Peak Summer Workshop. Ed: M. Sigwarth, ASP Conf. Ser., 236, 161-195.

Uitenbroek, H., 1989, *A&A*, 213, 360.

Uitenbroek, H., 2001, *ApJ*, 557, 389.

Vissers, J.G.M., Danilovic, S., de la Cruz Rodríguez, J., and 7 more, 2021, *A&A*, 645, 1.

Wedemeyer-Bohm, S.; Carlsson, M., 2011, *A&A*, 528, 1.